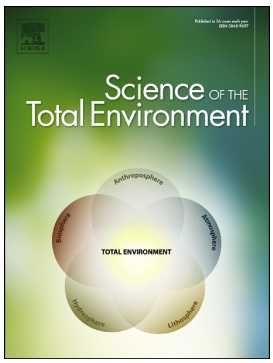

Integrated modeling of 2D urban surface and 1D sewer hydrodynamic processes and flood risk assessment of people and vehicles

Boliang Dong, Junqiang Xia, Meirong Zhou, Qijie Li, Reza Ahmadian, Roger A. Falconer

PII: S0048-9697(22)01190-1

DOI: https://doi.org/10.1016/j.scitotenv.2022.154098

Reference: STOTEN 154098

To appear in: *Science of the Total Environment*

Received date: 21 December 2021

Revised date: 18 February 2022

Accepted date: 19 February 2022

Please cite this article as: B. Dong, J. Xia, M. Zhou, et al., Integrated modeling of 2D urban surface and 1D sewer hydrodynamic processes and flood risk assessment of people and vehicles, *Science of the Total Environment* (2021), https://doi.org/10.1016/j.scitotenv.2022.154098

Integrated modeling of 2D urban surface and 1D sewer hydrodynamic processes and flood risk assessment of people and vehicles

Boliang Dong[1], Junqiang Xia[1,*] xiajq@whu.edu.cn, Meirong Zhou[1], Qijie Li[1], Reza Ahmadian[2], Roger A. Falconer[2,3]

[1]State Key Laboratory of Water Resources and Hydropower Engineering Science, Wuhan University, Wuhan 430072, China;
[2]School of Engineering, Cardiff University, Cardiff, CF24 3AA, UK
[3]Yangtze Institute for Conservation and Development, Hohai University, Nanjing 210024, China
[*]Corresponding author.

Abstract

In order to accurately simulate the whole urban flooding processes and assess the flood risks to people and vehicles in floodwaters, a 2D-surface and a 1D-sewer integrated hydrodynamic model was proposed in this study, with the module of flood risk assessment of people and vehicles being included. The proposed model was firstly validated by a dual-drainage laboratory experiment on the flood inundation process over a typical urban street, and the relative importance of model parameters and model uncertainties were evaluated using the GSA-GLUE method. Then the model was applied to simulate an actual urban flooding process that occurred in Glasgow, UK, with the influence of the sewer drainage system on flood inundation processes and hazard degree distributions of people and vehicles being comprehensively discussed. The following conclusions are drawn from this study: (i) The proposed model has a high degree of accuracy with the NSE values of key hydraulic variables greater than 0.8 and the GSA indicates that Manning roughness coefficients for surface and sewer flows, inlet weir and orifice discharge coefficients, are the most relevant parameters to influence the simulated results; (ii) vehicles are vulnerable to larger water depths while human stability is significantly influenced by higher flow velocities, with the overall flood risk of people being less than that of vehicles; and (iii) about 88.7% of the total inflow volume

was drained to the sewer network, and the sewer drainage system greatly reduced the flood risks to people and vehicles except the local areas with large inundation water depths, where the sewer drainage increased the local flow velocity leading to higher flood risks especially for people.

Keywords: urban flooding, integrated modeling, flood risk assessment, human safety, vehicle safety

1 Introduction

Flooding is one of the most destructive natural disasters in the world, which can not only threaten the safety of people and property but also lead to some social and environmental consequences (Michel-Kerjan and Kunreuther, 2011; Adnan et al., 2019a; Han and He, 2021). The flood risk of an area is closely related to the natural geographical features and infrastructure levels (Adnan et al., 2019b). Exceptionally heavy rainfall is identified as the main driver of extreme flooding events, and in some cases, the combined effect of extreme precipitation with river flood and storm surges will result in more catastrophic losses, especially for densely populated riverside or coastal cities (Adnan et al., 2020b; Zhang and Najafi, 2020). In recent years, due to the global climate change and the acceleration of human activities, the frequency and intensity of urban flooding disasters are rising, leading to a great challenge to urban flood prevention and reduction measures (Jacobson, 2011; Adnan et al., 2020a). Consequently, there has been a growing demand to improve the methods of flood risk analysis, in order to deal with the increasing probability and catastrophic results of flooding disasters (Apel et al., 2009; Ward et al., 2011).

The hazard degrees of people and vehicles have increased noticeably with the aggravation of urban flooding disasters. On 20 July 2021, the Jingguang Road Tunnel in Zhengzhou City, China was inundated, with 6 people being drowned and 247 vehicles being submerged (Mo, 2021). An

investigation into the hazard degrees of people and vehicles during urban flooding events can provide a scientific basis for flood hazard prevention and mitigation measures. Accurate prediction and evaluation of flood risk is the precondition of any strategies for disaster prevention and mitigation (Diaz-Nieto et al., 2012). The most widely used flood risk assessment methods are physically-based deterministic modeling approaches and probabilistic approaches (Di Baldassarre et al., 2010). Deterministic modeling approaches use physically-based hydrology and/or hydrodynamic models to assess the flood risks and do not take account of the uncertainties in the modelling process. As urban flooding disasters can be caused by a limited drainage capacity of linking elements or a limited capacity of drainage network systems, reflecting the interaction between surface runoff and underground pipe flow is crucial to urban flood modeling. In order to achieve simultaneous simulations of surface runoff and underground pipe flow, many numerical models based on the dual-drainage concept have been developed (Djordjević et al., 1999; Fraga et al., 2016; Nanía et al., 2015). Such models coupled a two-dimensional (2D) surface runoff module with a one-dimensional (1D) sewer flow module, and the interaction between these two models was achieved using the inlet/manhole discharge capacity formulas (Noh et al., 2016).

However, the uncertainty and chaotic nature of urban flooding processes lead to a great challenge to accurate numerical modeling (Freer et al., 2011). Actually, uncertainty can occur in almost every step of a deterministic urban flooding modeling study, including but not limited to model abstraction, input data quality, model parameter estimation, and correct initial and boundary conditions (Cea et al., 2011; Ozdemir et al., 2013; Montanari and Koutsoyiannis, 2014; Fernández-Pato et al., 2016). The presence of uncertainty and randomness should be properly addressed, by conducting the uncertainty and sensitivity analyses, using multiple models, or

combining the deterministic model with other probabilistic approaches, to obtain more reliable flood risk assessments (Villarini et al., 2010; Zhang and Najafi, 2020; Li et al., 2021).

In general, the hazard degrees of people and vehicles are related to flow characteristics including water depth and flow velocity, own physical features such as weight and height, and underlying surface conditions covering different ground slopes and surface roughness degrees (Russo et al., 2013; Xia et al., 2014b; Milanesi et al., 2016, p.; Martinez-Gomariz et al., 2018). Various formulas or criteria have been proposed based on experience, laboratory experiments, mechanical analysis, and combinations of mechanical analysis and laboratory experiments. Among them, the criteria based on both physical experiments and mechanical analysis can reflect the critical mechanical instability state, and therefore provide better university and accuracy. Intending to give a precise assessment of the hazard degree of people and vehicles during an urban flooding process, many researchers conducted numerical studies by coupling hydrodynamic models with the criterion of flood risk assessment. Xia et al. (2011) integrated a 2D surface runoff hydrodynamic model with the algorithms for assessing the flood hazard risks of different people groups and vehicles to simulate flash floods and presented corresponding hazard degrees. Kvocka et al. (2016) compared the performance of an empirically derived method and a physically-based flood hazard assessment method in assessing two extreme flood events. Based on the analysis of numerical results, suggest using the physically-based method to evaluate the flood risk in areas prone to extreme floods. Wang et al. (2021) coupled a graphics processing unit (GPU) accelerated shallow water equation model with physically-based instability criteria to establish a dynamic, convenient, and accurate risk assessment framework for people and vehicles in floodwaters. However, previous studies of flood risk assessment for people and vehicles mainly focused on surface flood processes,

and seldom discussed the influence of underground sewer systems on the surface flood inundation processes and the corresponding hazard degrees. Therefore, these models are difficult to be applied in actual urban environments.

In this study, an urban flooding modelling and hazard risk assessment framework that coupled a whole process hydrodynamic model for urban flooding and a hazard risk assessment module composed of physically-based incipient velocity formulas for people and vehicles in floodwaters was proposed. The performance of the proposed model was evaluated by a large-scale dual-drainage laboratory experiment. Then the model was used to simulate an urban flooding disaster that occurred in Glasgow, UK. By setting up a generalized sewer system, the effects were discussed of sewer drainage on the flood inundation process as well as corresponding flood risks to people and vehicles.

2 Description of the integrated model

This section introduces the surface and sewer coupled hydrodynamic modeling framework for urban floods, as well as the risk assessment module of people and vehicles in floodwaters. The total hydrodynamic modeling framework is composed of a 2D surface runoff module, a flow exchange module, and a sewer network module.

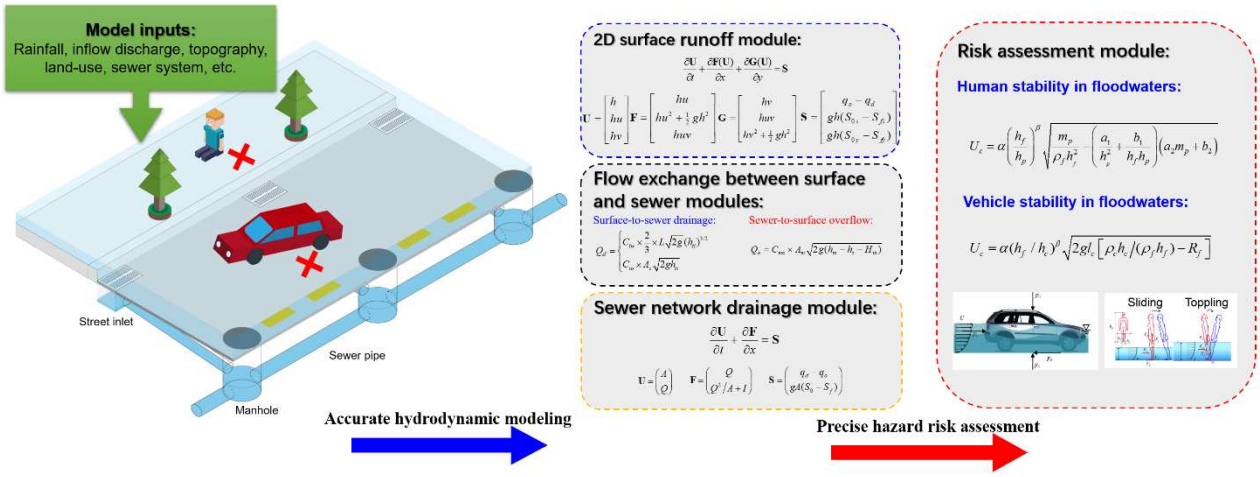

Figure 1 Flowchart of the 2D surface and 1D sewer coupled hydrodynamic module of urban flooding and flood risk assessment module.

2.1 Modeling framework for urban flood hydrodynamics

2.1.1 Module of 2D surface runoff

The depth-averaged 2D shallow water equations have been widely used in describing open-channel flows in rivers, coastal regions and urban areas (Lai, 2010; Ozdemir et al., 2013). The 2D SWEs are represented by three partial differential equations, which can be written in the following conservative form:

$$\frac{\partial \mathbf{U}}{\partial t}+\frac{\partial \mathbf{F}(\mathbf{U})}{\partial x}+\frac{\partial \mathbf{G}(\mathbf{U})}{\partial y}=\mathbf{S} \quad (1)$$

where **U** is the vector of conserved variables; **F** and **G** are flux vectors in the x and y coordinates; **S** is the source term including bed friction and bed slope. The above vectors can be written in detail as follows:

$$\mathbf{U}=\begin{bmatrix} h \\ hu \\ hv \end{bmatrix},\ \mathbf{F}=\begin{bmatrix} hu \\ hu^2+\frac{1}{2}gh^2 \\ huv \end{bmatrix},\ \mathbf{G}=\begin{bmatrix} hv \\ huv \\ hv^2+\frac{1}{2}gh^2 \end{bmatrix},\ \mathbf{S}=\begin{bmatrix} q_o-q_d \\ gh(S_{0x}-S_{fx}) \\ gh(S_{0y}-S_{fy}) \end{bmatrix} \quad (2)$$

where h is the water depth, u and v are the depth-averaged velocity components in the x and y coordinates; q_d and q_o are the drainage and overflow discharges per unit area, respectively; g is the gravitational acceleration; the bed slope term S_{0x} and S_{0y} accounts the variation of terrain elevation z_b in the x and y coordinates; S_{fx} and S_{fy} are the friction slopes in the x and y directions.

The surface runoff module adopts a cell-centered Godunov-type finite volume method to solve the 2D SWEs, in which the conserved variables are stored in the center of each cell. In the current model, the computational domain is divided into a set of triangular meshes to replicate the geometry. Numerical flux through the cell edge is calculated using the HLLC approximate Riemann solver.

Inappropriate discretization of source terms may influence mass conservation and numerical stability. In this study, the novel surface reconstruction method (SRM) proposed by Xia et al. (2017) is adopted to hydrostatically reconstruct the Riemann state across the cell edge, which can avoid limitations in traditional hydrostatic reconstruction implementations such as the "waterfall effect" and incorrect bed slope discretization where the topography is stiff or discontinuous (Hou et al., 2014). In the original study, the SRM method is developed for a kind of structured mesh, and it is extended to the unstructured triangular mesh in this study. It should be noted that numerical schemes based on the SRM are only first-order accuracy, and therefore, more computational cells are required to get the same performance than high-order schemes. However, as high-order schemes require more computational time per cell, first-order schemes with more computational cells may get better performance than high-order schemes with sparse spatial discretization under the same simulation time (Fernández-Pato et al., 2016).

2.1.2 Flow exchange between surface and sewer modules

The hydraulic performance of a linking structure such as manhole and street inlet can greatly affect the overall performance of a sewer drainage system (Leitão et al., 2017). Under normal conditions, surface runoff is intercepted by street inlets and discharged into underground sewer pipes (Gómez et al., 2019). If the sewer system is surcharged, the discharge capacity of the manhole-gully system may reduce, and even the sewer flow would overflow to the surface, once the water head of the sewer flow is higher than the ground surface. Therefore, an accurate characterization of the flow exchange is important in numerical models of urban flooding. For simplicity, the flow interaction between surface and sewer systems can be generalized into two patterns: the surface-to-sewer drainage process and the sewer-to-surface overflow process. In the

current module of flow exchange, it is assumed that the surface runoff is intercepted by street inlets, while the overflow process only occurs via manholes.

(1) Surface-to-sewer drainage process

The flow drainage process is usually described using the drainage capacity formulas based on the weir and/or orifice equations as a simplification (Rubinato et al., 2017; Martins et al., 2018; Palla et al., 2018). The drainage pattern of street inlet can be divided into submerged and non-submerged stages with an increase in surface water depth, which can be formulated respectively by the weir and orifice formula (Lee et al., 2012). Under small surface water depths, the drainage capacity of a street inlet is restricted by the capacity of the inlet grate. The increase in surface water depth will make the inlet grate to be fully submerged. In this situation, the overall discharge capacity is equal to the discharge capacity of the connection tube. The drainage discharge of the two processes can be characterized as follows:

$$Q_d = \begin{cases} C_{iw} \times \frac{2}{3} \times L\sqrt{2g}\,(h_s)^{3/2} & \text{Non-submerged} \\ C_{io} \times A_s \sqrt{2gh_{ti}} & \text{Submerged} \end{cases} \quad (3)$$

where Q_d is the drainage discharge; h_s is the surface water depth; h_{ti} is the hydraulic head difference between surface runoff and sewer pipe flow; A_s is the cross-sectional area of the side tube; L is the perimeter of the inlet grate; C_{iw} and C_{io} are the corresponding empirical coefficients for the weir and orifice formulae.

(2) Sewer-to-surface overflow process

Under sewer surcharge conditions, the total water head of sewer flow can be greater than the water head of surface runoff, which can cause the occurrence of sewer-to-surface overflow. This process is generally governed by the orifice formula in urban flooding models (Djordjević et al.,

2005), which can be given in this form:

$$Q_o = C_{mo} \times A_m \sqrt{2g(h_m - h_s - H_m)} \quad (4)$$

where Q_o is the overflow discharge; C_{mo} is the orifice coefficient of the manhole; A_m is the cross-sectional area of the manhole; h_m is the water head of the manhole; H_m is the height of the manhole (equalling the height from the ground surface to the bottom of the manhole).

2.1.3 Sewer network drainage module

Generally, sewers are designed to transport stormwater through ventilated pipes in a free-surface flow regime. Sewer surcharging may occur during heavy rainfall events, with the flow regime within the sewer pipes transiting between free-surface and pressurized flows. The cross-sectionally averaged continuity and momentum equations for sewer flows under free-surface and pressurized regimes can be written in a conservative form (Sanders and Bradford, 2011):

$$\frac{\partial \mathbf{U}}{\partial t} + \frac{\partial \mathbf{F}}{\partial x} = \mathbf{S} \quad (5)$$

where

$$\mathbf{U} = \begin{pmatrix} A \\ Q \end{pmatrix} \quad \mathbf{F} = \begin{pmatrix} Q \\ Q^2/A + I \end{pmatrix} \quad \mathbf{S} = \begin{pmatrix} 0 \\ gA(S_0 - S_f) \end{pmatrix} \quad (6)$$

where A is the wetted cross-sectional area of the sewer flow; Q is the discharge through the sewer pipe; I is the pressure term; S_0 is the slope of the sewer pipe; S_f is the friction head loss slope estimated using the Manning's equation.

The sewer network drainage module can be solved based on the 1D finite volume method framework. A sewer pipe is discretized into multiple uniform computational cells in numerical simulations. Numerical fluxes across cell edges are determined by solving the Riemann problem using the HLL approximate Riemann solver (Sanders and Bradford, 2011). The regime transition between free-surface flow and pressurized flow is calculated using the Preissmann slot method

(León et al., 2009; Kerger et al., 2011).

2.2 Module of flood risk assessment

The instability of people and vehicles has been the main cause of casualties during flood disasters (Doocy et al., 2013). In the risk assessment module, the mechanics-based and experimental calibrated incipient velocity formulas for flooded people and vehicles proposed by Xia et al., (2014a, b) are adopted to give a quantitative assessment of flood hazard degrees.

2.2.1 Criterion of human stability in floodwaters

Sliding (friction) instability and toppling (moment) instability are identified as the major instability mechanisms for people in floodwaters (Jonkman and Penning-Rowsell, 2008). Based on the comprehensive mechanical analysis, Xia et al. (2014a) proposed a formula to calculate the incipient velocity of people in floodwaters, which can be used to evaluate people's flood risk. In the case of small water depths and high flow velocities, the drag force of the flow can be greater than the effective friction force, which may lead to sliding instability. Under large water depths, the buoyancy force can greatly reduce the resisting moment of the effective bodyweight and cause the occurrence of toppling instability. However, as the sliding instability only occurred under conditions with very shallow water depth and large flow velocity which are seldom occurs in practice, Xia et al., (2014a) suggest using the toppling instability threshold to evaluate the flood hazard degree of people in floodwaters. The formula characterizing the incipient velocity in toppling instability can be written as Eq. (7):

$$U_c = \alpha \left(\frac{h_f}{h_p} \right)^{\beta} \sqrt{\frac{m_p}{\rho_f h_f^2} - \left(\frac{a_1}{h_p^2} + \frac{b_1}{h_f h_p} \right) \left(a_2 m_p + b_2 \right)} \quad (7)$$

where U_c is the incipient flow velocity; h_f is the water depth; h_p is the height of a human body; m_p is the weight of a human body; ρ_f is the density of water; α and β are empirical coefficients; a_1, b_1, a_2, b_2

are coefficients describing the feature of a human body (Xia et al., 2014a). Parameters in Eq. (7) are presented in Table 1.

Table 1 Parameters for the stability criterion of different people groups in floodwaters (Xia et al., 2014a).

Object	Parameters in Eq. (7)								
	h_p (m)	m_p (kg)	ρ_f (kg.m^{-3})	α m$^{0.5}$.s^{-1}	β -	a_1 -	b_1 -	a_2 m^3.kg^{-1}	b_2 m^3
Adult	1.7	60	1000	3.472	0.188	0.633	0.367	1.015×10^{-3}	-4.927×10^{-3}
Children	1.26	25.5	1000	3.472	0.188	0.633	0.367	1.015×10^{-3}	-4.927×10^{-3}

2.2.2 Criterion of vehicle stability in floodwaters

Vehicles parking on flooded streets can be swept away during extreme flood events, which may cause further threats to passengers, pedestrians, and urban infrastructures. Many experimental and analytical studies were conducted to investigate the stability of vehicles in floodwaters (Martinez-Gomariz et al., 2017; Shah et al., 2019). Floating instability and sliding instability are the most common instability patterns for flooded vehicles (Martinez-Gomariz et al., 2018). It is generally accepted that the stability of a flooded vehicle is related to the flow condition (water depth and velocity), vehicle characteristics (weight, shape), ground slope and orientation angle (the angle between flow direction and vehicle body). Xia et al. (2014b) analyzed the forces acting on a flooded vehicle and proposed a mechanics-based formula for the incipient velocity of vehicles in floodwaters. Based on scaled physical experiments, two key parameters of the derived formula were calibrated. The incipient velocity for vehicles in floodwaters can be written as:

$$U_c = \alpha (h_f / h_c)^{\beta} \sqrt{2gl_c \left[\rho_c h_c / (\rho_f h_f) - R_f \right]} \quad (8)$$

where h_c is the height of the vehicle; l_c is the length of the vehicle (it is assumed that the flow direction is parallel to the side of a vehicle); ρ_c is the density of the vehicle, $R_f = h_c\gamma_c/(h_k\gamma_f)$, in which h_k is the critical water depth at which the vehicle starts to float, γ_c and γ_f are the specific weights of

vehicle and water; α and β are empirical coefficients. Parameters for the stability criterion of different vehicles are presented in Table 2.

Table 2 Parameters for the stability criterion of different vehicles in floodwaters (Xia et al., 2014b).

Object	Parameters in Eq. (8)						
	h_c (m)	l_c (m)	ρ_c (kg.m^{-3})	α	β -	R_f -	h_k (m)
Honda Accord	1.48	4.945	170.44	0.212	-0.562	0.65	0.45
Audi Q7	1.737	5.089	203	0.438	-0.219	0.551	0.67

2.2.3 Quantification method of flood hazard degree

Fig. 2 shows the depth-incipient velocity curve for different people groups and vehicles in floodwaters. Following the same method as the previous numerical studies on flood risk assessment (Xia et al., 2011; Kvocka et al., 2018), the hazard degrees of people and vehicles can be expressed by the ratio of the actual flow velocity u_f to incipient velocity U_c:

$$HD = \min(1.0, u_f / U_c) \quad (9)$$

where HD is the hazard degree. If the flow velocity is significantly lower than the incipient velocity, the hazard degree will be close to zero, which means the overall hazard degree is relatively low. If the actual flow velocity is close to or larger than the incipient velocity of people or vehicles, the flood hazard degree will be close to 1, indicating a high flood risk.

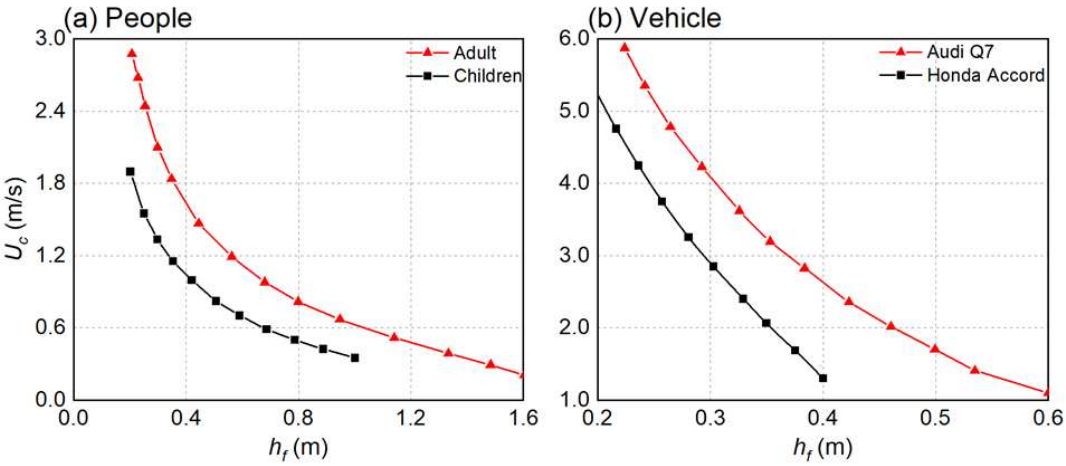

Figure 2 Depth-incipient velocity curves: (a) different people groups; (b) different vehicles.

3 Results

In this section, the accuracy of the proposed model was first validated by the results of a large-scale dual-drainage laboratory experiment concerning flash flood inundation processes over a typical urban street. Then the validated model was applied to simulate a real urban flooding process that occurred in Glasgow, UK.

3.1 Model validation using a dual-drainage laboratory experiment

3.1.1 Description of the laboratory experiment and numerical model setup

Experimental data obtained from the laboratory platform with a real urban street structure were selected to validate the current model. The platform was constructed based on a large-scale flume located in North China University of Water Resources and Electric Power (Dong et al., 2021). As illustrated in Fig. 3, the flume is 20.5 m in length, 3 m in width, and 0.6 m in height. A dam located 4.5 m from the upstream sidewall separates the flume into the reservoir zone and the downstream model urban zone. The model main road is located in the center of the flume, and buildings, sidewalks as well as street inlets are symmetrically distributed on both sides. A drainage network is located under the laboratory flume, which is composed of rain boxes, side tubes, and main sewer

pipe. At the start of each experiment test, the gate of the reservoir was lifted rapidly and then the flood inundated along the whole street. Ultrasonic water level gauges were used to measure the surface water level variations at seven specific positions. Ten electromagnetic flowmeters and a pressure gauge were respectively used to measure the drainage discharge through the street inlets and the water depth variation in the main sewer pipe. The distance between the pressure gauge and the last pair of side tubes is set to 1.0 m. In this study, the computational domain was divided into 52, 516 unstructured triangular meshes with a spatial resolution of 5 cm. The downstream of the flume was specified as the free boundary condition while other boundaries were specified as the solid wall boundary conditions.

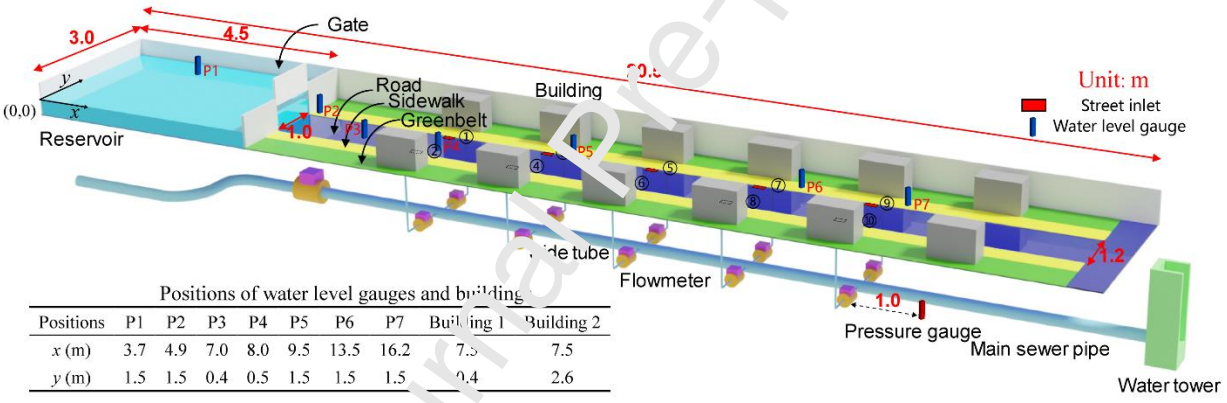

Positions of water level gauges and building

Positions	P1	P2	P3	P4	P5	P6	P7	Building 1	Building 2
x (m)	3.7	4.9	7.0	8.0	9.5	13.5	16.2	7.5	7.5
y (m)	1.5	1.5	0.4	0.5	1.5	1.5	1.5	0.4	2.6

Figure 3 Sketch of the laboratory platform for flash flood inundation and positions of measurement points.

3.1.2 Sensitivity analysis

The proposed model included a comprehensive representation of the dual-drainage urban flooding process. However, the model performance is affected by various uncertainties, especially parameter uncertainties (Di Baldassarre et al., 2010). Sensitivity analysis can identify the most influential input parameters to the simulated results and therefore can facilitate the model application. In this section, a global sensitivity analysis method of the extended Fourier amplitude sensitivity test (E-FAST) (Saltelli et al., 1999) was selected to identify the most influential parameters. By adopting

the E-FAST method, main and total effects for the influence of one parameter on the overall model outputs can be obtained. The model outputs covered the NSE values (Nash and Sutcliffe, 1970) of the surface water depth variation at the measurement point P6 and the sewer water depth variation. Five model inputs were selected to conduct sensitivity analysis and the description of the selected input parameters and the corresponding variation ranges are presented in Table 3.

For the E-FAST global sensitivity analysis method, a total of $N_p \times N_{MC}$ model runs were required where N_p was the number of input parameters selected for GSA and N_{MC} was the number of Monte Carlo simulations per parameter. In the current study, N_{MC} was set to 500 corresponding to a total of 2500 model simulations. The main and total effects sensitivity indices on NSE of each model input parameter are presented in Fig. 4. For the surface water depth variation at P6, the variables of surface roughness (n) and inlet orifice coefficient (C_o), were identified as the most influential parameters since these parameters directly influenced the flood inundation processes and controlled the drainage volume from the surface to the underground sewer network. As the underground sewer network presented a ventilated state, the sewer flow had little influence on the surface processes. Therefore, the sensitivity of sewer pipe roughness (n_p) was small. In terms of the simulated sewer water depth variation, surface roughness (n), inlet weir and orifice coefficient (C_w and C_o), and roughness of sewer pipe (n_p), were found to have a significant effect. The wet-dry threshold water depth (h_{min}) was found to be non-influential to the variation in surface and sewer water depths, and this parameter can be treated as a constant in numerical simulations.

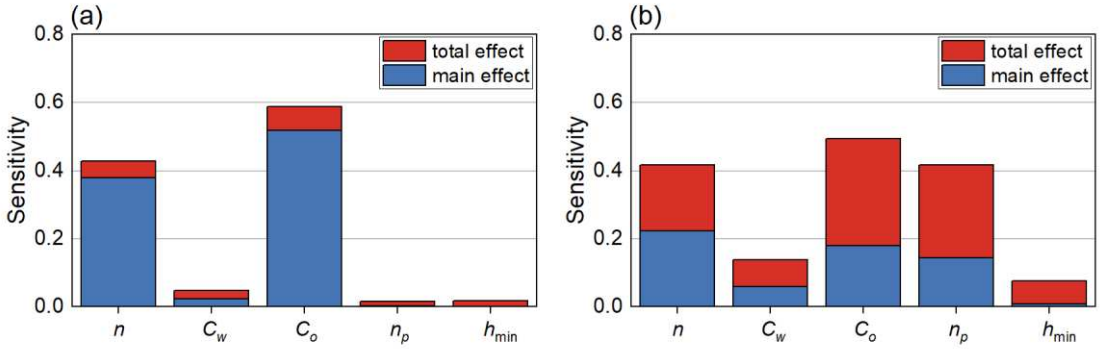

Figure 4 Results from the sensitivity analysis for the selected model parameters: (a) variation in surface water depth at P6; (b) variation in sewer water depth.

Table 3 Variation ranges of input parameters for sensitivity analysis

Order	Symbol	Description	Unit	Min	Max
1	n	Surface roughness	$s.m^{-1/3}$	0.008	0.013
2	C_o	Inlet orifice coefficient	-	0.01	0.6
3	C_w	Inlet weir coefficient	-	0.01	0.6
4	n_p	Pipe roughness	$s.m^{-1/3}$	0.008	0.013
5	h_{min}	Wet–dry threshold water depth	m	1E-6	0.001

3.1.3 Simulated results and uncertainty analysis

Uncertainty analysis was conducted using the GSA-GLUE method (Ratto et al., 2001) that combines the widely used generalized likelihood uncertainty estimation (GLUE) (Beven and Freer, 2001) and the GSA. Following the GSA-GLUE framework, the input parameter sample set generated for the E-FAST analysis was applied for the GLUE analysis. In this study, the threshold likelihood of NSE > 0.1 was used to get the behavioral solution samples. Fig. 5 compares the laboratory observations with the uncertainty bands with the bounds of 95% confidence interval and the best-fit results calculated using the global optimal parameters. In general, the model presents satisfactory accuracy with most of the measured data points within the bounds of uncertainty bands and the NSE coefficients of the best-fit results greater than 0.94 and 0.81 for the surface and sewer water depth variations, respectively. The overall uncertainty of the calculated sewer water depth variation was

greater than that of the surface water depth. In addition, the uncertainty in surface water depth variation increased from upstream to downstream, with the coverage of measured data within the bounds of the 95% confidence interval reducing from 87% at P2 to 73% at P7. It should be mentioned that only the parameter uncertainty was discussed while other sources of uncertainty in the initial and boundary conditions or model structural errors were not considered. Therefore, more detailed uncertainty analyses should be conducted in the future to provide a comprehensive understanding of the uncertainty in 1D-2D coupled urban flooding modeling.

Figure 5 Comparisons between the calculated and experimental data: (a-c) surface water depth hydrographs at points P2, P4, and P7; (d) variation in the water depth of the main sewer pipe.

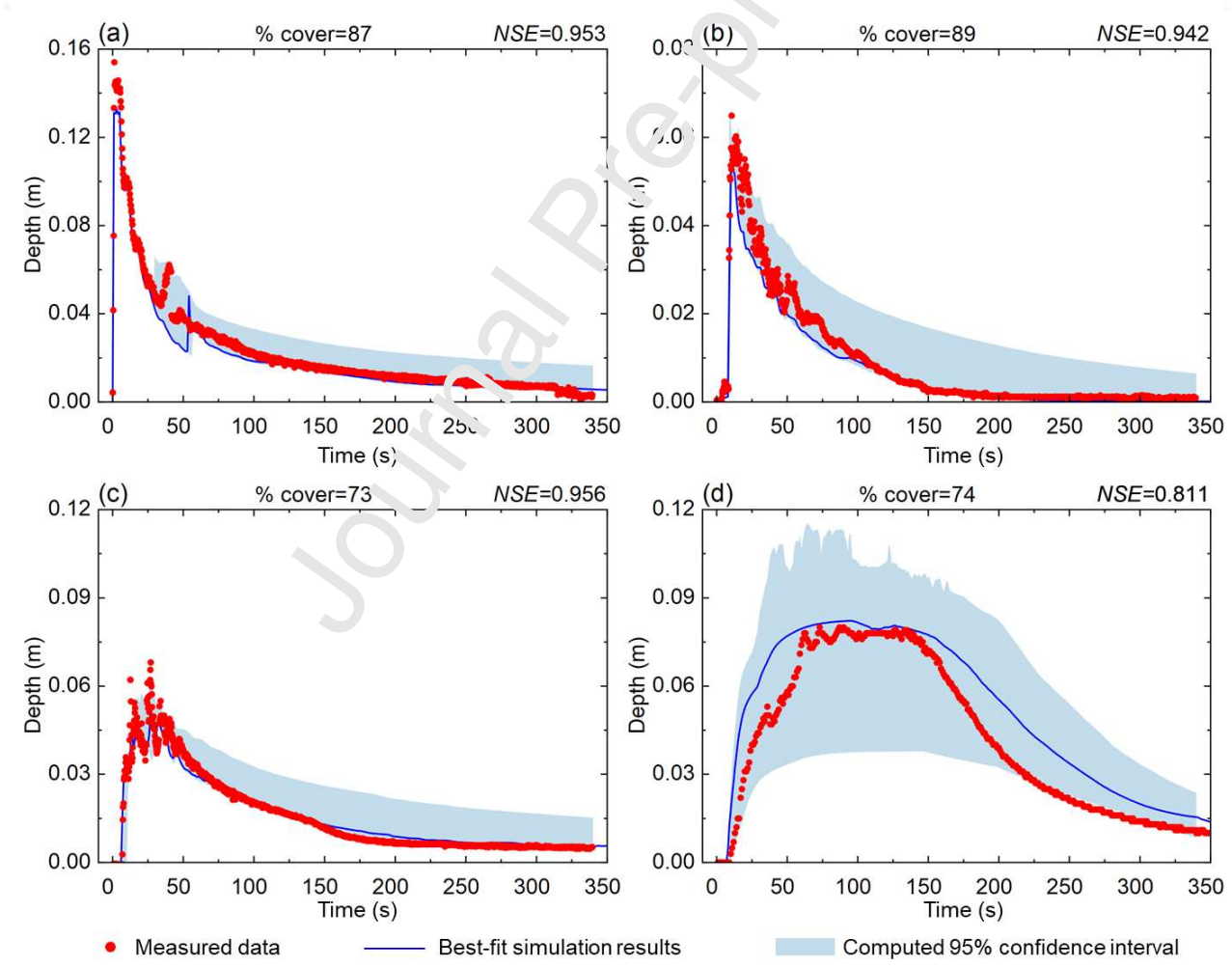

3.2 Simulation of Glasgow flood

3.2.1 Description of the study area and the flood event

Hunter et al. (2008) proposed a 2D hydraulic model benchmark for urban flooding based on a flood event that occurred in a small urban catchment within Glasgow city, Scotland, UK. This benchmark is based on a real flood event that occurred on 30 July 2002, with the violent streamflow caused by heavy rainfall overflowing from the culvert located at the location Q in Fig. 6 (Hunter et al., 2008). Therefore, this urban flood event was generalized as a phenomenon of overflowing from a source point. As the catchment area upstream of the location Q is small, the flood event responds rapidly to rainfall and presents a sharp rise and fall in discharge hydrograph. The inflow discharge hydrograph reconstructed based on the eyewitness reports and historical photographs is shown in Fig. 6, with the maximum discharge and the total overflow volume being 10 m^3/s and 8600 m^3, respectively. During the flood event, the flood inundated alone the two east-west oriented streets with low water depths and high flow velocities, finally ponding in the region around the point STA3. However, this benchmark dataset included only the comprehensive surface topography data, and the sewer system data were not covered, such as sizes and locations of street inlets, manholes and sewer pipes. To investigate the interaction between surface runoff and sewer pipe flow as well as the corresponding influence on hazard degrees of people and vehicles, a hypothetical sewer drainage system was used in this study. The hypothetical drainage was composed of 146 street inlets, 50 manholes, and 49 sewer pipes. Street inlets and sewer pipes were arranged along the roads from northwest to southeast. The interaction between surface runoff and sewer pipe flow is achieved through the inlet-manhole approach, which suggests that surface runoff is drained through multiple street inlets into the nearest manhole (Jang et al., 2018). A uniform slope of 0.4% was set to all

sewer pipes and the elevation of the sewer network outlet was set to 21.0 m. The diameter of all sewer pipes was set to 1.2 m and the planform geometry of each street inlet was set to 0.45 m×0.75 m.

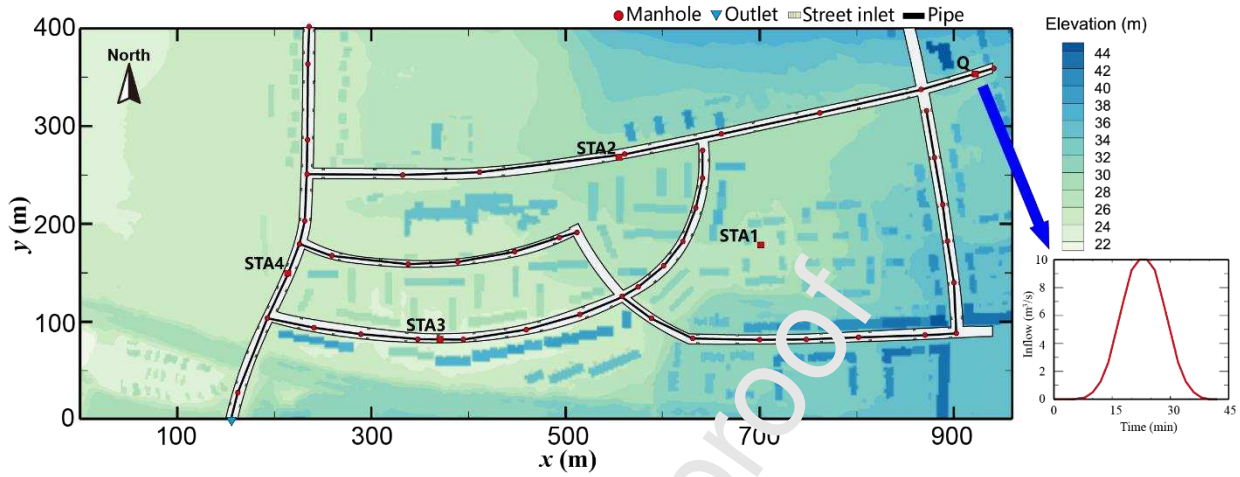

Figure 6 Topography and sewer drainage system structure of the study area.

3.2.2 Model setup for the urban flood in Glasgow

The computational domain had a rectangular shape with 1.0 km in length and 0.4 km in width. The underlying topography of the catchment was derived from a combination of airborne laser altimetry (LiDAR) and digital map data with a 2 m spatial resolution. DEM cells inside building vectors were artificially raised to represent the building height and ensure that would not be submerged during an urban flood event. As the DEM data provided a detailed characterization of the boundary of buildings, all the buildings were reflected using the building-block method (Schubert and Sanders, 2012). The whole computational domain was divided into about 898, 330 unstructured triangular meshes with a special resolution of about 1 m. All the boundaries of the computational domain were specified as the solid wall boundary condition. Constant Manning roughness coefficients for the ground surface and the sewer network pipes were specified as 0.020 and 0.012 $s.m^{-1/3}$, respectively. The pressurized wave speed a of sewer flow varies in time and space,

depending on the entrainment of air (Sanders and Bradford, 2011), which causes the coefficient hard to determine. According to numerical experiments on the sensitivity of pressurized wave speed, different wave speed values can exert little influence on the overall results (Li et al., 2020). However, a larger wave speed will lead to numerical oscillations and significantly influence computational efficiency. As suggested by Sanders and Bradford, (2011), the pressurized flow wave speed was set to 75 m/s. The weir and orifice coefficients for the drainage of street inlets were set to 0.44 and 0.54, respectively; the overflow orifice coefficient of manholes was set to 0.20.

3.2.3 Simulated results

Fig. 7 presents the spatial and temporal variations of the flood inundation process. At about t = 2400 s, the study area reached the maximum inundation degree, with the maximum water depth of about 0.8 m. Subsequently, the inundation range, as well as the water depth, gradually decreased due to the drainage of the sewer system. From t =6000 s to t = 7200 s, the surface runoff around street inlets was almost drained, and therefore, the influence of the sewer system on the water depth distribution was insignificant during this period, with only a small amount of water remaining in low-lying areas.

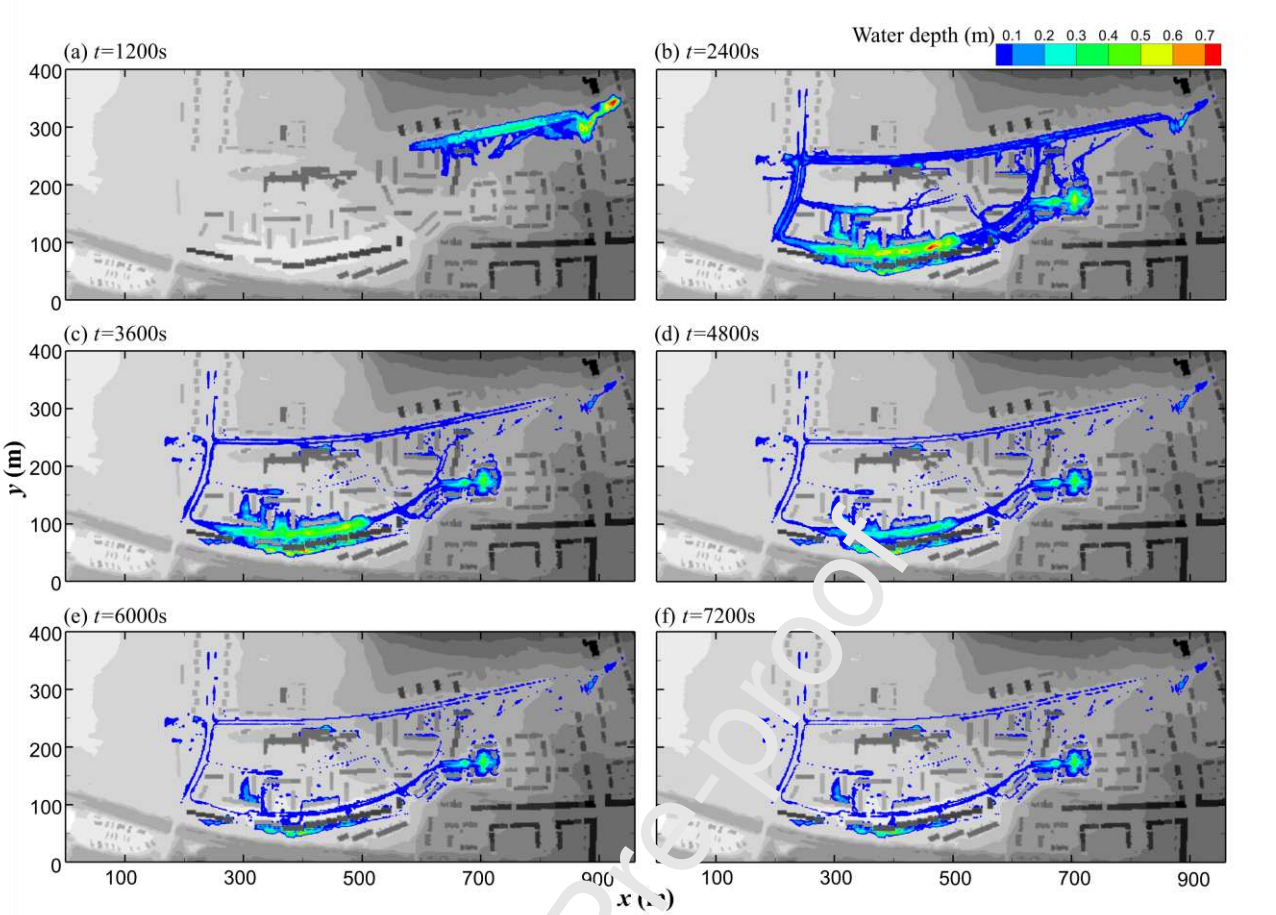

Figure 7 Spatial and temporal variation of the flood inundation process.

Fig. 8 shows the variations in water volume hydrographs at different parts of the computation domain. The sewer system plays an important role in the flood inundation process, with the total sewer drainage volume being about 7635 m^3 accounting for 88.7% of the total inflow volume. The maximum inundation volume directly influences the distribution of water depth and therefore influences the hazard degree of a flooded area. At t =1900 s, the surface water volume reached the maximum value. In this case, the maximum surface inundation volume was about 4950 m^3, representing a reduction of 44% compared with the case without the sewer drainage. At t = 1420 s to 2000 s, the water volume stored in the sewer system was almost unchanged, while the surface volume presented a continuously increasing trend, indicating the sewer system had reached the maximum drainage capacity.

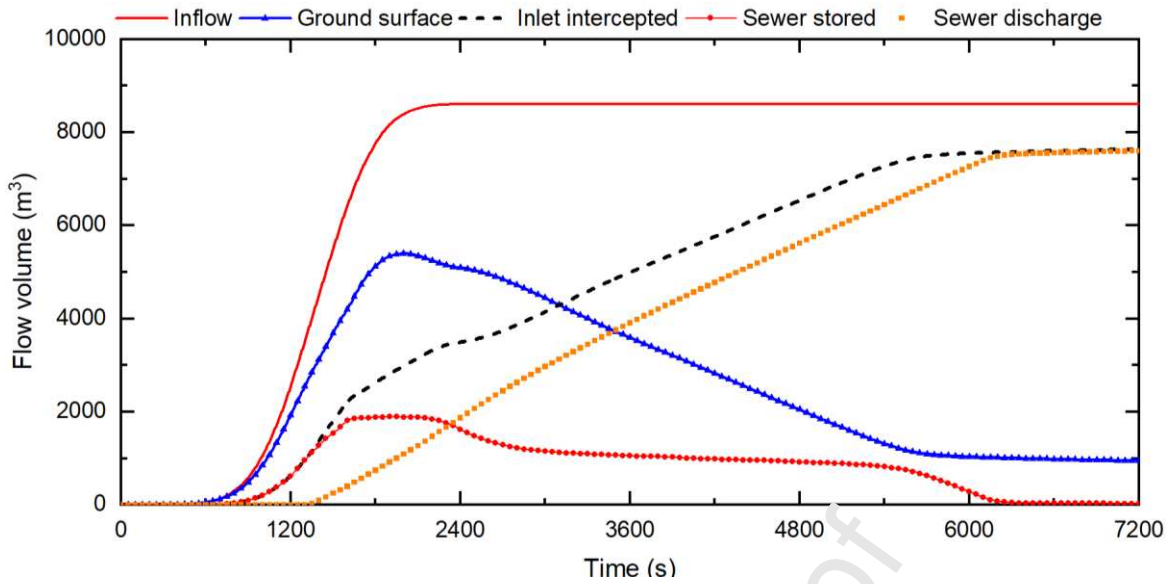

Figure 8 Temporal variations in water volumes of total inflow, surface flow, inlet intercepted, sewer stored and accumulated sewer drainage.

Because of the rapid falling of surface runoff, the flow regime transition between open channel flow to pressurized flow may occur in sewer systems (Vasconcelos et al., 2006). Once the sewer water head was higher than the ground elevation of the study area, the sewer flow would overflow into the surface. As mentioned in section 2, surface runoff is intercepted by street inlets and discharged into the sewer network via connected manholes in the current model. While the sewer flow can only overflow through the manholes. The accumulated exchange volumes through different manholes are presented in Fig. 9. The spatial distribution of accumulated exchange volumes was significantly affected by the location of manholes. Most of the surface runoff was incepted by street inlets located at the upstream side of the study area and was conveyed to the sewer outlet via the sewer pipes. The discharge within sewer pipes increased from upstream to downstream and therefore exceeded the discharge capacity of the sewer pipes, which led to the occurrence of sewer surcharge. In conclusion, the interaction between surface runoff and sewer pipe flow is a complex process. It is necessary to consider not only the discharge capacity of street inlets

but also the drainage capacity of sewer networks. Directly simplifying the sewer drainage system as a set of street inlets is hard to meet the acquirement of simulating actual urban flooding processes.

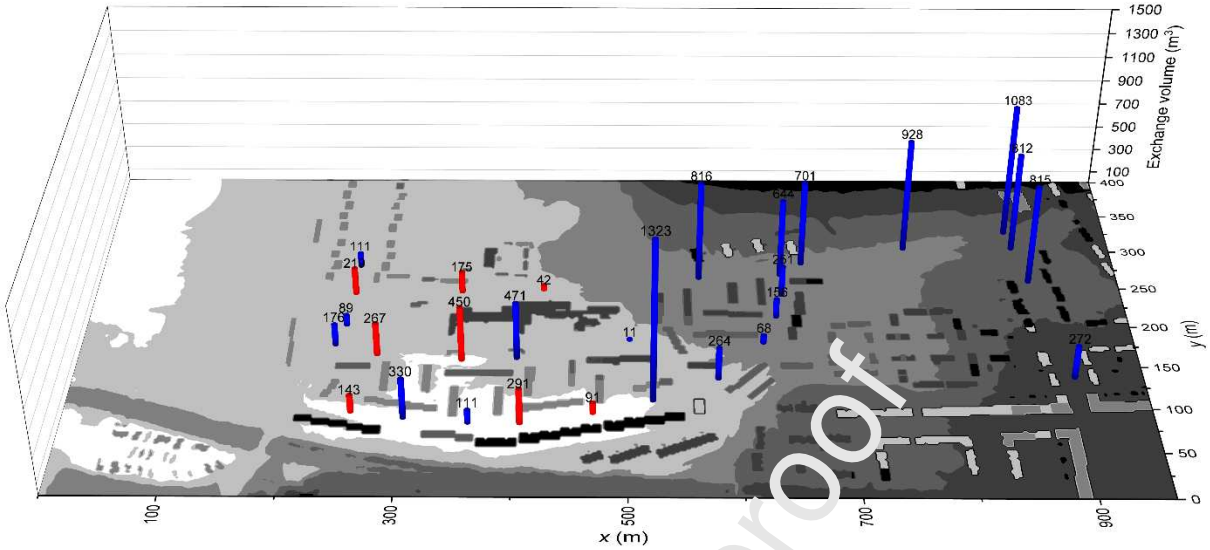

Figure 9 Spatial distribution of accumulated exchange volume between the surface and the sewer network through different manholes. (blue bars: accumulated drainage volume; red bars: accumulated overflow volume)

4 Discussion

In this section, the influences were discussed of the underground sewer system on the flood inundation characteristics as well as corresponding hazard degrees for different people groups and vehicles.

4.1 Influence of the sewer system on flood inundation characteristics

Water depth and flow velocity are two key parameters to evaluate the hazard degrees during flood events (Kreibich et al., 2009). Fig. 10 presents the comparisons of maximum water depths and velocities under the scenarios with and without the sewer drainage system. The main street located on the southwest of the computational domain had the maximum inundation degree, with the water depth values being close to 0.8 m. Because the inflow discharge in the initial stage was much larger than the drainage capacity of the sewer drainage system, the distributions of flood inundation range

and maximum flow velocity under these two scenarios were almost the same. However, as time increased, the cumulative impact of the sewer drainage system became apparent, and the flooded area with a larger inundation water depth (h>0.7) was significantly reduced under the with sewer drainage system scenario.

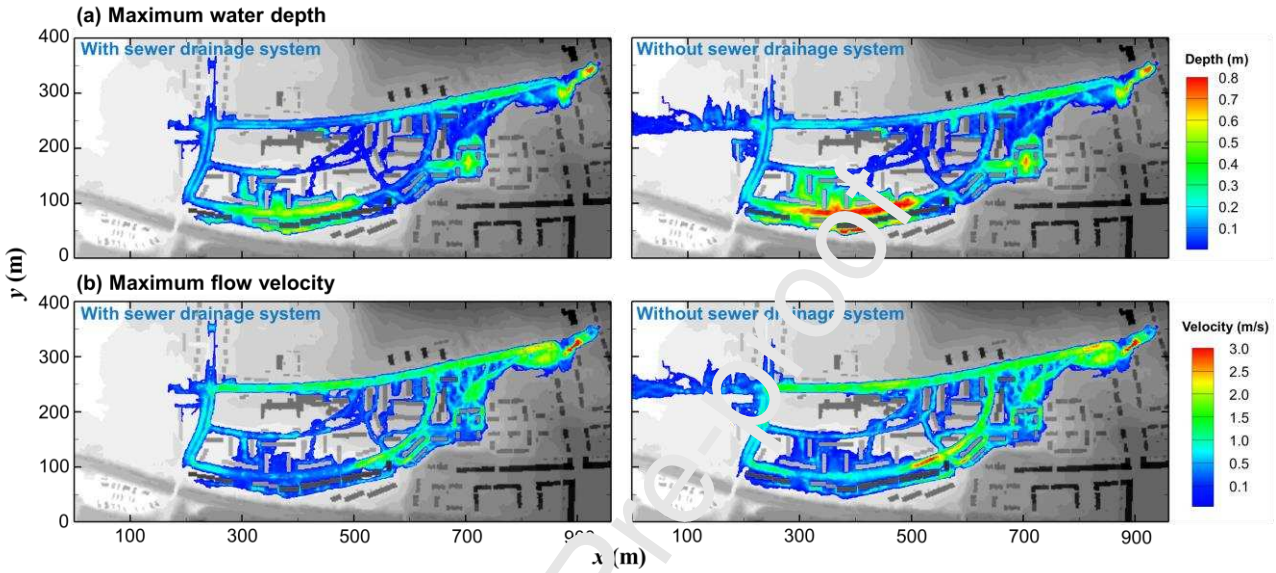

Figure 10 Distributions of maximum water depth and flow velocity under the scenarios with and without the sewer drainage system: (a) maximum water depth; (b) maximum flow velocity.

Fig. 11 illustrates the water depth hydrographs at points STA1-4. Point STA1 is located near the inflow point and represents a zone that can rapidly accumulate the water at the beginning of the simulation. As there are no drainage structures around STA1, the water depth variations under these two scenarios were almost the same during the whole process. STA2 is located in the middle of the road which can receive the water from east to west. During the flood inundation process, surface runoff was intercepted and conveyed through street inlets, which slightly reduced the water depth and delayed the flood wave speed. STA3 and STA4 are located in the lower part of the study area, which can receive the water from the road network, and therefore present as a ponding at the end of the simulation. Due to the influence of the sewer system, points STA3 and STA4 were almost dry at

t = 6000 s and t = 3600 s, respectively. At points STA2 and STA4, the sewer system reduced the flow velocity, while the flow velocity at STA3 increased from t = 3600 s to t = 7200 s as a result of the sewer drainage. Therefore, for flooded areas with larger inundation water depths, the sewer

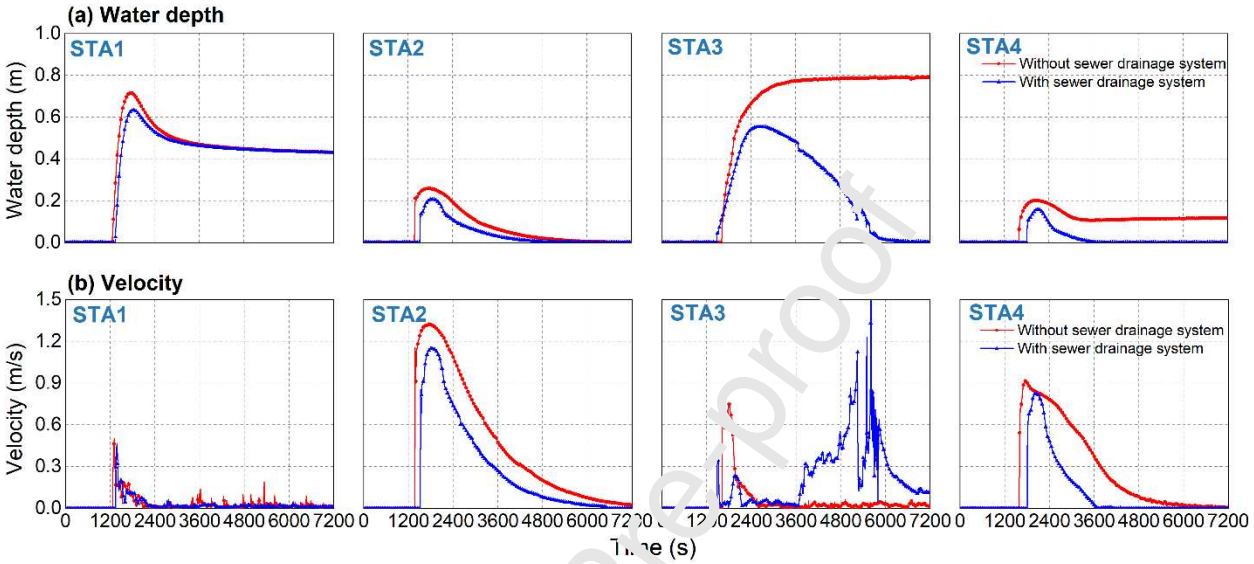

drainage system may increase the local velocity of surface flow and lead to potential hazard risks.

Figure 11 Comparisons of water depth and flow velocity hydrographs at different points under the scenarios with and without the sewer drainage system.

4.2 Influence of the sewer system on hazard degrees

Based on the high-resolution spatial and temporal hydrodynamic results, the corresponding hazard degrees for people and vehicles were evaluated using the module of flood risk assessment of people and vehicles. This section highlights the influence of the urban sewer drainage system on flood hazard degrees. Fig. 12 presents a comparison of maximum hazard degree distributions of different people groups and vehicles. As a result of high velocity and large water depth, the children would face a great threat on the main roads of the study area. However, the hazard degree of adults was relatively small in the whole study area except the location being near the inflow point. The

sewer system showed little influence on the hazard degree of adults, with the flood risk distributions under the scenarios with and without the sewer drainage being almost the same. People and vehicles presented different characteristics of hazard degree distributions in this study. The flood risk of vehicles was higher, and the distribution of maximum hazard degree for vehicles was almost the same as the distribution of water depth. As the sewer system significantly reduced the surface water depth, the hazard degree of vehicles would be greatly mitigated, especially for the vehicle of Audi Q7.

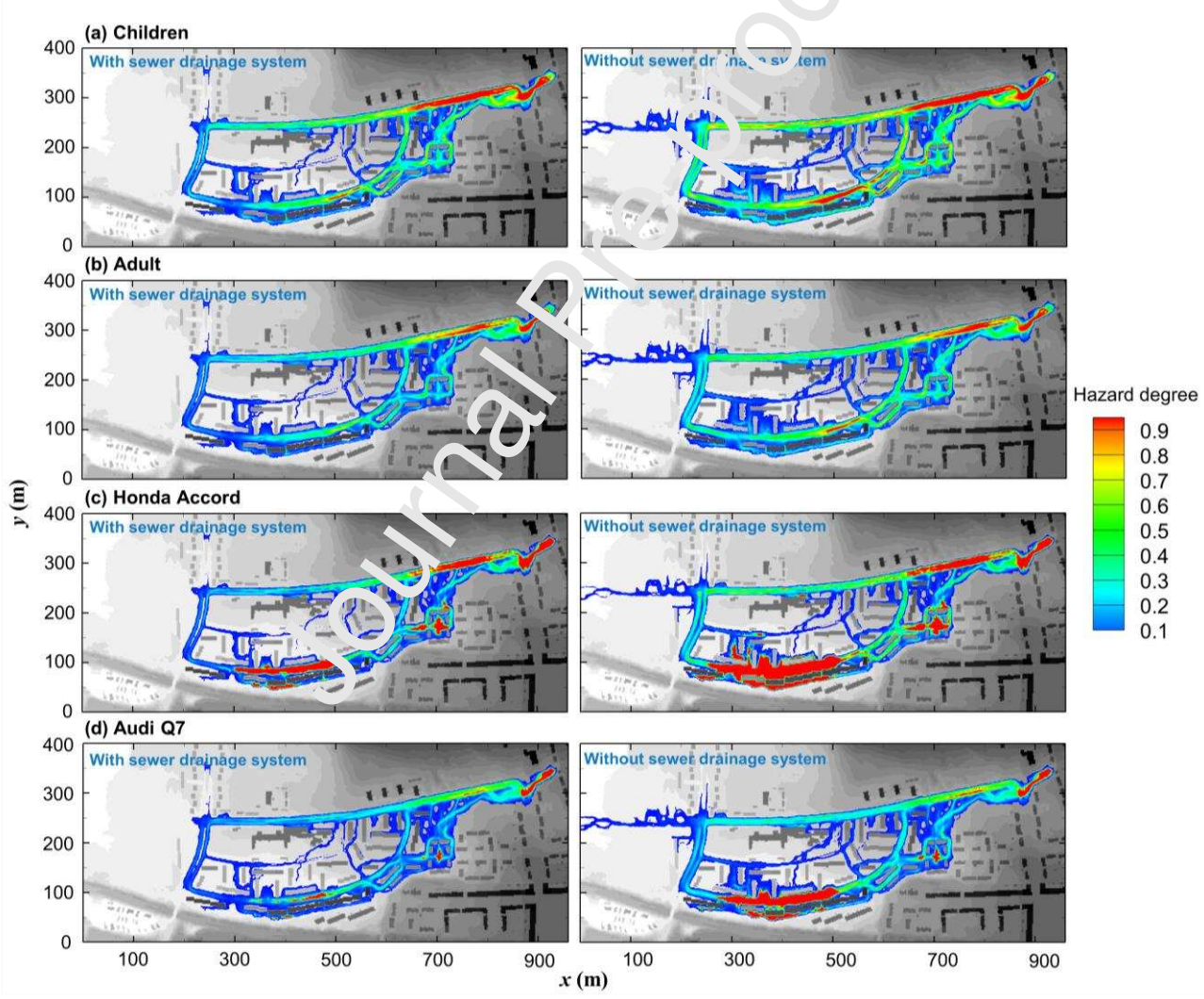

Figure 12 Comparisons of maximum hazard degree distributions of different people groups and vehicles under the scenarios with and without the sewer drainage system.

Fig. 13 presents a comparison of hazard degree variations for different vehicles and different people groups under the scenarios with and without the sewer drainage system. In most cases, the sewer system mitigated the flood risks of people and vehicles, with the maximum hazard degrees and high-risk time (hazard degree greater than 0.9) significantly being reduced. As points STA1 and STA2 are located at the upstream side of the study area, the impact of the sewer drainage system is relatively small, and the temporal variations of hazard degree under these two scenarios were almost the same. During the flood inundation process, a large amount of water was drained into the sewer network through street inlets. The flow drainage process not only reduced the water depth but also slowed down the flow velocity, and hence the flood hazard degrees of people and vehicles in floodwaters were greatly affected. At point STA3, the high-risk time of Honda Accord under the scenario with the sewer drainage system lasted only about 2100 s, while under the scenario without the sewer drainage system, the high-risk time lasted from t = 1850 s to the end of the simulation. For the vehicle of Audi Q7, the maximum hazard degree at STA3 was equal to 0.519 because the water depth was greatly reduced by the sewer drainage system. The sewer drainage process increased the flood risk of people at STA3. For the scenario with the sewer drainage system, the maximum flood risks of children and adults after t = 3600 s were 0.228 and 0.156, respectively. While the values were 0.172 and 0.088, respectively for the scenario without the sewer drainage system. The reason for this phenomenon is that under larger water depth circumstances, topping instability that a human body pivots around the heel is the main instability mode. Topping instability was observed to occur under the condition of large water depth and small flow velocity, and therefore the stability thresholds are sensitive to the variation in flow velocity. The drainage process increased the flow velocity around STA3, therefore leading to higher flood hazard risks. But

the hazard degrees of children and adults were relatively low, and additional flood risk caused by the sewer drainage was negligible under this circumstance.

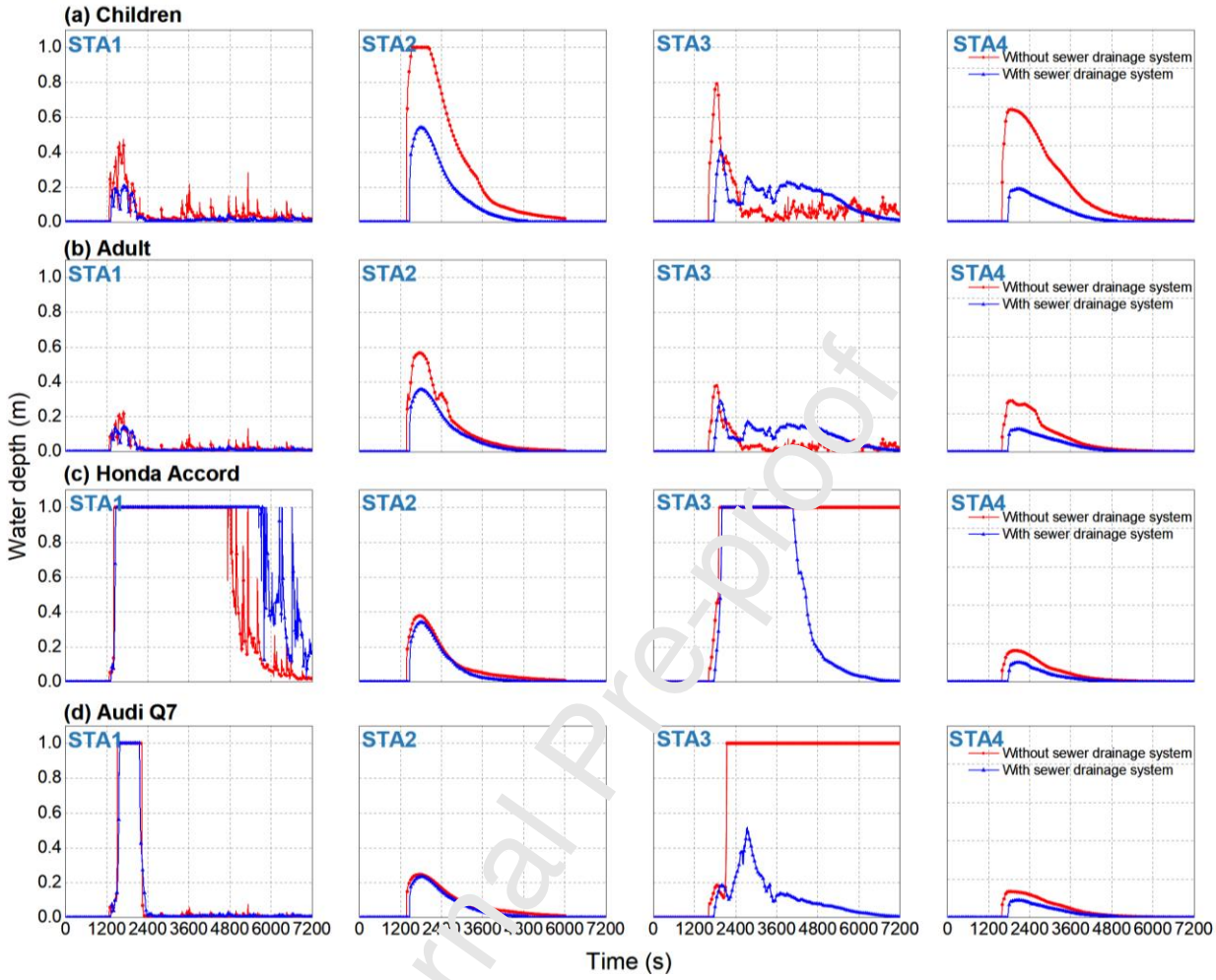

Figure 13 Comparisons of hazard degree variations for different vehicles and people groups under the scenarios with and without the sewer drainage system.

5 Conclusions

In this study, a surface and sewer coupled hydrodynamic model was proposed, with the module of flood risk assessment of people and vehicles being included. The proposed model was first validated by a laboratory experiment of flood inundation in a flume with model uncertainty and input parameter sensitivity were analyzed using the GSA-GLUE method. Then the model was applied to simulate a flash flood event that occurred in Glasgow, UK. The influences of urban sewer

drainage systems on flood inundation processes and corresponding hazard degrees of people and vehicles were quantitively discussed. The following conclusions are obtained from this study:

(i) The proposed model can accurately simulate the urban flooding process, including the surface runoff inundation, flow exchange between surface runoff and sewer pipe flow, and flow drainage through the sewer network. Model predictions were in close agreement with the observations in a laboratory experiment, with the NSE values of key hydrodynamic parameters greater than 0.8 for the best-fit simulation results.

(ii) E-FAST analysis indicates that the variables of surface roughness (n), inlet orifice coefficient (C_o) were identified as the key parameters to influence the variation in surface water depth variation. For the sewer water depth variation, the parameters of surface roughness (n), inlet weir and orifice coefficient (C_w and C_o), the roughness of sewer pipe (n_p) were found to have a significant effect. The wet-dry threshold water depth (h_{min}) was found to be non-influential to the variation in surface and sewer water depths, and this parameter can be treated as a constant in numerical simulations.

(iii) For urban flood hazards, road networks are the main path for flood inundation and therefore become high-risk areas for people and vehicles. Vehicles are more vulnerable to large water depths while the stability of a human body is more sensitive to high flow velocity, and therefore people and vehicles present different characteristics of hazard degree distribution in an urban area.

(iv) According to the simulated results of the Glasgow flood event, about 8107 m^3 of water was drained to the sewer system, which accounted for 94.8% of the total inflow volume. Urban drainage systems can effectively mitigate the urban flooding disaster in terms of reducing the inundation water depth, slowing down the flow velocity, and therefore reducing the hazard degrees of people and vehicles. However, for flooded areas with large water depths, the drainage process may increase

the local velocity, which may lead to potential hazard risks.

Acknowledgments

This work was funded by the National Natural Science Foundation of China (Grant Nos. 51725902, 41890820); the Royal Academy of Engineering through the Urban Flooding Research Policy Impact Programme (Grant No. UUFRIP\100031); and the Newton Advanced Fellowships from the NSFC and the UK Royal Society (Grant Nos. 52061130219; NAF\R1\201156).

CRediT author statement

21-12-2021

Subject: Integrated modeling of 2D urban surface and 1D sewer hydrodynamic processes and flood risk assessment of people and vehicles

Boliang Dong: Methodology, Investigation, Writing - Original Draft. **Junqiang Xia*:** Resources, Methodology, Writing - Review & Editing. **Meirong Zhou:** Conceptualization, Formal analysis**.** **Qijie Li:** Writing - Review & Editing. **Reza Ahmadian:** Funding acquisition. **Roger A. Falconer:** Writing - Review & Editing.

Declaration of interests

The authors declare that they have no known competing financial interests or personal relationships that could have appeared to influence the work reported in this paper.

The authors declare the following financial interests/personal relationships which may be considered as potential competing interests

References

Adnan, M.S.G., Abdullah, A.Y.M., Dewan, A., Hall, J.W., 2020a. The effects of changing land use and flood hazard on poverty in coastal Bangladesh. Land Use Policy 99, 104868. https://doi.org/10.1016/j.landusepol.2020.104868

Adnan, M.S.G., Dewan, A., Zannat, K.E., Abdullah, A.Y.M., 2019a. The use of watershed geomorphic data in flash flood susceptibility zoning: a case study of the Karnaphuli and Sangu river basins of Bangladesh. Natural Hazards 99, 425–448. https://doi.org/10.1007/s11069-019-03749-3

Adnan, M.S.G., Haque, A., Hall, J.W., 2019b. Have coastal embankments reduced flooding in Bangladesh? Science of The Total Environment 682, 405–416. https://doi.org/10.1016/j.scitotenv.2019.05.048

Adnan, M.S.G., Talchabhadel, R., Nakagawa, H., Hall, J.W., 2020b. The potential of Tidal River Management for flood alleviation in South Western Bangladesh. Science of The Total Environment 731, 138747. https://doi.org/10.1016/j.scitotenv.2020.138747

Apel, H., Aronica, G.T., Kreibich, H., Thieken, A.H., 2009. Flood risk analyses—how detailed do we need to be? Natural Hazards 49, 79–98. https://doi.org/10.1007/s11069-008-9277-8

Cea, L., Bermúdez, M., Puertas, J., 2011. Uncertainty and sensitivity analysis of a depth-averaged water quality model for evaluation of Escherichia Coli concentration in shallow estuaries. Environmental Modelling & Software 26, 1526–1539. https://doi.org/10.1016/j.envsoft.2011.08.001

Di Baldassarre, G., Schumann, G., Bates, P.D., Freer, J.E., Beven, K.J., 2010. Flood-plain mapping: a critical discussion of deterministic and probabilistic approaches. Hydrological Sciences Journal 55, 364–376. https://doi.org/10.1080/02626661003683389

Diaz-Nieto, J., Lerner, D.N., Saul, A.J., Blanksby, J., 2012. GIS Water-Balance Approach to Support Surface Water Flood-Risk Management. Journal of Hydrologic Engineering 17, 55–67. https://doi.org/10.1061/(ASCE)HE.1943-5584.0000416

Djordjević, S., Prodanović, D., Maksimović, C., 1999. An approach to simulation of dual drainage. Water Science and Technology 39, 95–103. https://doi.org/10.2166/wst.1999.0451

Djordjević, S., Prodanović, D., Maksimović, Č., Ivetić, M., Savić, D., 2005. SIPSON – Simulation of Interaction between Pipe flow and Surface Overland flow in Networks. Water Science and Technology 52, 275–283. https://doi.org/10.2166/wst.2005.0143

Dong, B., Xia, J., Zhou, M., Deng, S., Ahmadian, R., Falconer, R.A., 2021. Experimental and numerical model studies on flash flood inundation processes over a typical urban street. Advances in Water Resources 147, 103824. https://doi.org/10.1016/j.advwatres.2020.103824

Doocy, S., Daniels, A., Murray, S., Kirsch, T.D., 2013. The human impact of floods: a historical review of events 1980-2009 and systematic literature review. PLoS currents 5. https://doi.org/10.1371/currents.dis.f4deb457904936b07c09daa98ee8171a

Fernández-Pato, J., Caviedes-Voullième, D., García-Navarro, P., 2016. Rainfall/runoff simulation with 2D full shallow water equations: Sensitivity analysis and calibration of infiltration parameters. Journal of Hydrology 536, 496–513. https://doi.org/10.1016/j.jhydrol.2016.03.021

Fraga, I., Cea, L., Puertas, J., Suárez, J., Jiménez, V., Jácome, A., 2016. Global Sensitivity and GLUE-Based Uncertainty Analysis of a 2D-1D Dual Urban Drainage Model. Journal of Hydrologic Engineering 21, 04016004. https://doi.org/10.1061/(ASCE)HE.1943-5584.0001335

Freer, J., Beven, K.J., Neal, J., Schumann, G., Hall, J., Bates, P., 2011. Flood risk and uncertainty, in: Risk and Uncertainty Assessment for Natural Hazards. pp. 190–233. https://doi.org/10.1017/CBO9781139047562.008

Gómez, M., Russo, B., Tellez-Alvarez, J., 2019. Experimental investigation to estimate the discharge coefficient of a grate inlet under surcharge conditions. Urban Water Journal 16, 85–91. https://doi.org/10.1080/1573062X.2019.1634107

Han, J., He, S., 2021. Urban flooding events pose risks of virus spread during the novel coronavirus (COVID-19) pandemic. Science of The Total Environment 755, 142491. https://doi.org/10.1016/j.scitotenv.2020.142491

Hou, J., Simons, F., Liang, Q., Hinkelmann, R., 2014. An improved hydrostatic reconstruction method for shallow water model. Journal of Hydraulic Research 52, 432–439. https://doi.org/10.1080/00221686.2013.858648

Hunter, N.M., Bates, P.D., Neelz, S., Pender, G., Villanueva, I., Wright, N.G., Liang, D., Falconer, R.A., Lin, B., Waller, S., Crossley, A.J., Mason, D.C., 2008a. Benchmarking 2D hydraulic models for urban flooding. Proceedings of the Institution of Civil Engineers - Water Management 161, 13–30. https://doi.org/10.1680/wama.2008.161.1.13

Hunter, N.M., Bates, P.D., Neelz, S., Pender, G., Villanueva, I., Wright, N.G., Liang, D., Falconer, R.A., Lin, B., Waller, S., Crossley, A.J., Mason, D.C., 2008b. Benchmarking 2D hydraulic models for urban flooding. Proceedings of the Institution of Civil Engineers - Water Management 161, 13–30. https://doi.org/10.1680/wama.2008.161.1.13

Jacobson, C.R., 2011. Identification and quantification of the hydrological impacts of imperviousness in urban catchments: A review. Journal of Environmental Management 92, 1438–1448. https://doi.org/10.1016/j.jenvman.2011.01.018

Jang, J.-H., Chang, T.-H., Chen, W.-B., 2018. Effect of inlet modelling on surface drainage in coupled urban flood simulation. Journal of Hydrology 562, 168–180. https://doi.org/10.1016/j.jhydrol.2018.05.010

Jonkman, S.N., Penning-Rowsell, E., 2008. Human Instability in Flood Flows [1]. JAWRA Journal of the American Water Resources Association 44, 1208–1218. https://doi.org/10.1111/j.1752-1688.2008.00217.x

Kerger, F., Archambeau, P., Erpicum, S., Dewals, B.J., Pirotton, M., 2011. An exact Riemann solver and a Godunov scheme for simulating highly transient mixed flows. Journal of Computational and Applied Mathematics 235, 2030–2040. https://doi.org/10.1016/j.cam.2010.09.026

Kreibich, H., Piroth, K., Seifert, I., Maiwald, H., Kunert, U., Schwarz, J., Merz, B., Thieken, A.H., 2009. Is flow velocity a significant parameter in flood damage modelling? Natural Hazards and Earth System Sciences 9, 1679–1692. https://doi.org/10.5194/nhess-9-1679-2009

Kvocka, D., Ahmadian, R., Falconer, R.A., 2018. Predicting Flood Hazard Indices in Torrential or Flashy River Basins and Catchments. Water Resources Management 32, 2335–2352. https://doi.org/10.1007/s11269-018-1932-6

Kvocka, D., Falconer, R.A., Bray, M., 2016. Flood hazard assessment for extreme flood events. Natural Hazards 84, 1569–1599. https://doi.org/10.1007/s11069-016-2501-z

Lai, Y.G., 2010. Two-Dimensional Depth-Averaged Flow Modeling with an Unstructured Hybrid Mesh. Journal of Hydraulic Engineering 136, 12–23. https://doi.org/10.1061/(ASCE)HY.1943-7900.0000134

Lee, S., Nakagawa, H., Kawaike, K., Zhang, H., 2012. Study on inlet discharge coefficient through the different shapes of storm drains for urban inundation analysis. Journal of Japan Society of Civil Engineers, Ser. B1 (Hydraulic Engineering) 68, I_31-I_36. https://doi.org/10.2208/jscejhe.68.I_31

Leitão, J.P., Simões, N.E., Pina, R.D., Ochoa-Rodriguez, S., Onof, C., Sá Marques, A., 2017. Stochastic evaluation of the impact of sewer inlets' hydraulic capacity on urban pluvial flooding. Stochastic Environmental Research and Risk Assessment 31, 1907–1922. https://doi.org/10.1007/s00477-016-1283-x

León, A.S., Ghidaoui, M.S., Schmidt, A.R., García, M.H., 2009. Application of Godunov-type schemes to transient mixed flows. Journal of Hydraulic Research 47, 147–156. https://doi.org/10.3826/jhr.2009.3157

Li, J., Cao, Z., Borthwick, A.G.L., 2021. Uncertainty quantification in shallow water-sediment flows: A stochastic Galerkin shallow water hydro-sediment-morphodynamic model. Applied Mathematical Modelling 99, 458–477. https://doi.org/10.1016/j.apm.2021.06.031

Li, Q., Liang, Q., Xia, X., 2020. A novel 1D-2D coupled model for hydrodynamic simulation of flows in drainage networks. Advances in Water Resources 137, 103519. https://doi.org/10.1016/j.advwatres.2020.103519

Martinez-Gomariz, E., Gomez, M., Russo, B., Djordjevic, S., 2018. Stability criteria for flooded vehicles: a state-of-the-art review. Journal of Flood Risk Management 11, S817–S826. https://doi.org/10.1111/jfr3.12262

Martinez-Gomariz, E., Gomez, M., Russo, B., Djordjevic, S., 2017. A new experiments-based methodology to define the stability threshold for any vehicle exposed to flooding. Urban Water Journal 14, 930–939. https://doi.org/10.1080/1573062X.2017.1301501

Martins, R., Rubinato, M., Kesserwani, G., Leandro, J., Djordjević, S., Shucksmith, J.D., 2018. On the Characteristics of Velocities Fields in the Vicinity of Manhole Inlet Grates During Flood Events. Water Resources Research 54, 6408–6422. https://doi.org/10.1029/2018WR022782

Michel-Kerjan, E., Kunreuther, H., 2011. Redesigning Flood Insurance. Science 333, 408–409. https://doi.org/10.1126/science.1202616

Milanesi, L., Pilotti, M., Bacchi, B., 2016. Using web-based observations to identify thresholds of a person's stability in a flow. Water Resources Research 52, 7793–7805. https://doi.org/10.1002/2016WR019182

Mo, H., 2021. Measures needed to minimize risk [WWW Document]. URL http://www.ecns.cn/news/society/2021-08-03/detail-ihaptpct3741141.shtml (accessed 2.18.22).

Montanari, A., Koutsoyiannis, D., 2014. Modeling and mitigating natural hazards: Stationarity is immortal! Water Resources Research 50, 9748–9756. https://doi.org/10.1002/2014WR016092

Nanía, L.S., León, A.S., García, M.H., 2015. Hydrologic-Hydraulic Model for Simulating Dual Drainage and Flooding in Urban Areas: Application to a Catchment in the Metropolitan Area of Chicago. Journal of Hydrologic Engineering 20, 04014071. https://doi.org/10.1061/(ASCE)HE.1943-5584.0001080

Nash, J.E., Sutcliffe, J.V., 1970. River flow forecasting through conceptual models part I — A discussion of principles. Journal of Hydrology 10, 282–290. https://doi.org/10.1016/0022-1694(70)90255-6

Noh, S.J., Lee, S., An, H., Kawaike, K., Nakagawa, H., 2016. Ensemble urban flood simulation in comparison with laboratory-scale experiments: Impact of interaction models for manhole, sewer pipe, and surface flow. Advances in Water Resources 97, 25–37. https://doi.org/10.1016/j.advwatres.2016.08.015

Ozdemir, H., Sampson, C.C., de Almeida, G.A.M., Bates, P.D., 2013. Evaluating scale and roughness effects in urban flood modelling using terrestrial LIDAR data. Hydrology and Earth System Sciences 17, 4015–4030. https://doi.org/10.5194/hess-17-4015-2013

Palla, A., Colli, M., Candela, A., Aronica, G.T., Lanza, L.G., 2018. Pluvial flooding in urban areas: the role of surface drainage efficiency: The role of surface drainage on pluvial flooding. Journal of Flood Risk Management 11, S663–S676. https://doi.org/10.1111/jfr3.12246

Rubinato, M., Martins, R., Kesserwani, G., Leandro, J., Djordjević, S., Shucksmith, J., 2017. Experimental calibration and validation of sewer/surface flow exchange equations in steady and unsteady flow conditions. Journal of Hydrology 552, 421–432. https://doi.org/10.1016/j.jhydrol.2017.06.024

Russo, B., Gómez, M., Macchione, F., 2013. Pedestrian hazard criteria for flooded urban areas. Natural Hazards 69, 251–265. https://doi.org/10.1007/s11069-013-0702-2

Saltelli, A., Tarantola, S., Chan, K.P.-S., 1999. A Quantitative Model-Independent Method for Global Sensitivity Analysis of Model Output. Technometrics 41, 39–56. https://doi.org/10.1080/00401706.1999.10485594

Sanders, B.F., Bradford, S.F., 2011. Network Implementation of the Two-Component Pressure Approach for Transient Flow in Storm Sewers. Journal of Hydraulic Engineering 137, 158–172. https://doi.org/10.1061/(ASCE)HY.1943-7900.0000293

Schubert, J.E., Sanders, B.F., 2012. Building treatments for urban flood inundation models and implications for predictive skill and modeling efficiency. Advances in Water Resources 41, 49–64. https://doi.org/10.1016/j.advwatres.2012.02.012

Shah, S.M.H., Mustaffa, Z., Martinez-Gomariz, E., Kim, D.K., Yusof, K.W., 2019. Criterion of vehicle instability in floodwaters: past, present and future. International Journal of River Basin Management 1–23. https://doi.org/10.1080/15715124.2019.1566240

Vasconcelos, J.G., Wright, S.J., Roe, P.L., 2006. Improved Simulation of Flow Regime Transition in Sewers: Two-Component Pressure Approach. Journal of Hydraulic Engineering 132, 553–562. https://doi.org/10.1061/(ASCE)0733-9429(2006)132:6(553)

Villarini, G., Krajewski, W.F., Ntelekos, A.A., Georgakakos, K.P., Smith, J.A., 2010. Towards probabilistic forecasting of flash floods: The combined effects of uncertainty in radar-rainfall and flash flood guidance. Journal of Hydrology, Flash Floods: Observations and Analysis of Hydrometeorological Controls 394, 275–284. https://doi.org/10.1016/j.jhydrol.2010.02.014

Wang, N., Hou, J., Du, Y., Jing, H., Wang, T., Xia, J., Gong, J., Huang, M., 2021. A dynamic, convenient and accurate method for assessing the flood risk of people and vehicle. Science of The Total Environment 797, 149036. https://doi.org/10.1016/j.scitotenv.2021.149036

Ward, P.J., de Moel, H., Aerts, J.C.J.H., 2011. How are flood risk estimates affected by the choice of return-periods? Natural Hazards and Earth System Sciences 11, 3181–3195. https://doi.org/10.5194/nhess-11-3181-2011

Xia, J., Falconer, R.A., Lin, B., Tan, G., 2011. Numerical assessment of flood hazard risk to people and vehicles in flash floods. Environmental Modelling & Software 26, 987–998. https://doi.org/10.1016/j.envsoft.2011.02.017

Xia, J., Falconer, R.A., Wang, Y., Xiao, X., 2014a. New criterion for the stability of a human body in floodwaters. Journal of Hydraulic Research 52, 93–104. https://doi.org/10.1080/00221686.2013.875073

Xia, J., Falconer, R.A., Xiao, X., Wang, Y., 2014b. Criterion of vehicle stability in floodwaters based

on theoretical and experimental studies. Natural Hazards 70, 1619–1630. https://doi.org/10.1007/s11069-013-0889-2

Zhang, Y., Najafi, M.R., 2020. Probabilistic Numerical Modeling of Compound Flooding Caused by Tropical Storm Matthew Over a Data-Scarce Coastal Environment. Water Resources Research 56. https://doi.org/10.1029/2020WR028565

Graphical abstract

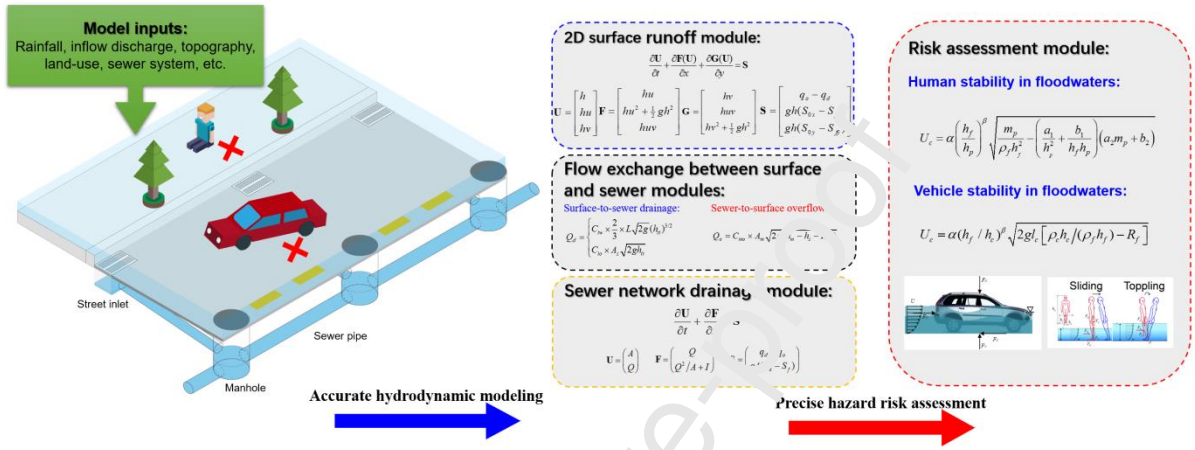

Highlights

- An integrated modeling framework was proposed of 2D surface and 1D sewer flows
- Incipient velocity formulas were used to assess flood risks of people and vehicles
- The model accuracy was validated using a dual-drainage laboratory experiment
- The effect was revealed of the sewer system on flood inundation and hazard degrees
- Results can be used to improve urban flood management and reduction measures